

Cite this: DOI: 00.0000/xxxxxxxxxx

Lanthanide molecular nanomagnets as probabilistic bits[†]Gerlitz M. Gutiérrez-Finol,^a Silvia Giménez-Santamarina,^a Ziqi Hu,^a Lorena E. Rosaleny,^a Salvador Cardona-Serra,^a Alejandro Gaita-Ariño,^{*a}Received Date
Accepted Date

DOI: 00.0000/xxxxxxxxxx

Over the decades, the spin dynamics of a large set of lanthanide complexes have been explored. Lanthanide-based molecular nanomagnets are bistable spin systems, generally conceptualized as classical bits, but many lanthanide complexes have also been presented as candidate quantum bits (qubits). Here we offer a third alternative and model them as probabilistic bits (p-bits), where their stochastic behaviour constitutes a computational resource instead of a limitation. Employing a novel modelling tool for molecular spin p-bits and molecular nanomagnets, we simulate a minimal p-bit network under realistic conditions. Finally, we go back to a recent systematic data gathering/recently published dataset and screen the best lanthanide complexes for p-bit behaviour, lay out the performance of the different lanthanide ions and chemical families and offer some chemical design considerations.

1 Introduction

The rising of Artificial Intelligence (AI) has been instrumental for pattern recognition¹, reasoning under uncertainty², control methods³, analyzing and classifying big data.^{4,5} Nevertheless, there is a need for scalable and energy-efficient hardware constructed following the same scheme: further progress of AI algorithms depends on the efficiency of its hardware.⁶ In this scenario, Neuromorphic Computing promises higher efficiency since it manipulates information with hardware processes that directly mimic the nature of neurons instead of emulating this via software.^{7,8}

The majority of current computers store and process information using deterministic bits that can take one of two possible values, 0 or 1. On the other hand, quantum computers are based on quantum-bits (qubits) which can exist in a superposition of $|0\rangle$ and $|1\rangle$ spin states described by a complex wavefunction.⁹ Between these two approaches, and sharing some of their qualities, we can find the probabilistic bits (p-bits, see Figure 1).¹⁰ These information elements can fluctuate stochastically between 0 and 1, but take a well-defined classical value at any given time.

There are many important advantages for the use of p-bits in computing.¹¹ In contrast with qubits, p-bits may operate at room temperatures with current technology, and yet are able to emulate sign-problem-free Hamiltonians (the so-called “stoquas-

tic” problems).¹² Furthermore, there are no hard physical limitations in terms of strength or distance of connections between p-bits as they can be wired employing known transistor technology. In fact, probabilistic computers are designed as a network of p-bits, autonomously fluctuating between 0 and 1, with probabilities that are controlled through an input constructed from the outputs of other p-bits.¹³ Recent landmarks of probabilistic computing include experimental integer factorisation using stochastic magnetic tunnel junctions,¹⁴ and an experimental spintronic demonstration employing the inherently stochastic behaviour of nanomagnets to implement probabilistic computing.^{15,16}

The nanomagnets employed as p-bits have so far been conventional, solid state materials. This is despite of three decades of research in molecular nanomagnets which have resulted in the theoretical investigation of the switching dynamics of stochastic nanomagnets, describing their relaxation time mechanisms¹⁷; in addition, many studies have been carried on in the area of the experimental characterisation of several hundreds of molecules presenting a measurable magnetic memory at low temperatures,¹⁸ with some of them being very promising as qubits.¹⁹ These systems deserve exploration for their use as nanoscale p-bits. Two challenges hampered the practical application of molecular nanomagnets as bits and qubits: (a) the difficulty to detect and manipulate a single molecular spin, and (b) the instability of their spin states, since the bit becomes useless as soon as a spin state suffers spontaneous changes and thus, information is lost. Qubits, the quantum version of spin-based memories, are even more challenging, requiring the preservation of quantum coherence and the implementation of coherent quantum operations.^{20,21} Notable achievements have been reported in both fields, such as molec-

^a Instituto de Ciencia Molecular (ICMol), Universitat de València, Paterna, Spain; E-mail: gaita@uv.es

[†] Electronic Supplementary Information (ESI) available: full technical details of the modelling and extensive screening of the SIMDAVIS dataset. See DOI: 10.1038/s41467-022-35336-9.

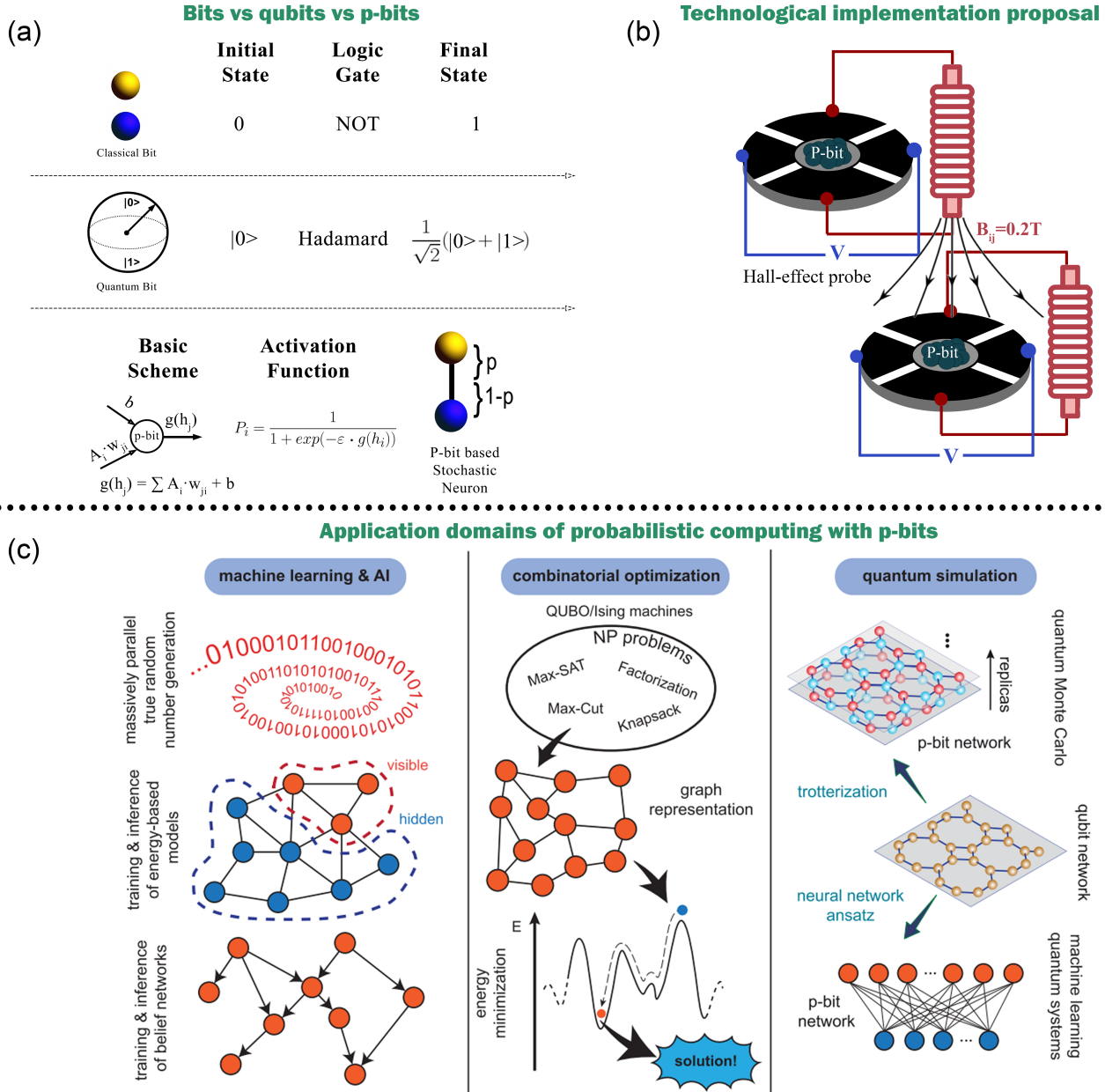


Fig. 1 (a) Bits vs qubit vs p-bit based stochastic neurons. For any starting state and logical operation, bits take simple 0 or 1 values, while qubits can take coherent superposition states $\alpha|0\rangle + \beta|1\rangle$. The operation is inherently deterministic, and the same memory position hold the initial and the final states. P-bit based Binary Stochastic Neurons function in layers (as neural networks) rather than by applying logic gates to memory positions. Furthermore, they are inherently stochastic, meaning two identical executions will result in different microscopic values for each neuron. (b) Proposed experimental setup for spin-based p-bits: the state of a p-bit i is read out by a Hall effect probe, and the resulting output voltage is amplified and translated a magnetic field that (after being properly weighted and added to all other signals) acts as input to a p-bit j . (c) Application domains of probabilistic computing with p-bits (reused with permission from Chowdhury et al,¹⁰ CC BY 4.0).

ular classical bits with (vanishingly thin) magnetic hysteresis up to liquid nitrogen temperature,^{22,23} or molecular qubits where one can implement a minimal quantum algorithm.²⁴ Although the ephemeral nature of spin information continues to be a problem and hinders further progress for these proposed computation technologies,^{19,25} there have been advances regarding the experimental implementation of quantum gates,^{26,27} and recent progress in the integration of molecular systems with superconducting circuits.^{28,29}

When molecular nanomagnets are considered as p-bits, their stochasticity is a crucial aspect of their nature rather than a defect to be corrected. Then, one can profit from the sophisticated modelling of their spin dynamics.³⁰ Initial studies on molecular nanomagnets assumed that a simple Orbach process was the main relaxation mechanism at high temperatures, thus the focus was set on modelling the effective barrier (U_{eff}),³¹ with a Quantum Tunneling of the Magnetisation (QTM) model being responsible for spin relaxation at low temperatures.³²

As sufficient data were gathered, the key role of other relaxation mechanisms, in particular Raman, was recognized. In parallel, spin-phonon coupling was found to be a key phenomenon, both for Orbach and for Raman processes, and became the focus of attention in the field.^{33–35} Recently, the data-science approach also provided some insights and pointers for the design of molecular nanomagnets.¹⁸ Combining electronic structure calculations with Machine Learning Force Fields is now allowing to unravel the nature of both the Orbach and the Raman relaxation pathways in terms of atomistic processes.³⁶

How could one leverage this expertise for the design of modes of computing based on molecular p-bits? Molecular nanomagnets in this context would act as Low Barrier Nanomagnets (LBNs) and be employed as Binary Stochastic Neurons (BSNs, see Figure 1).³⁷ BSNs would be the Artificial Neural Networks (ANNs)³⁸ equivalents of p-bits:

the output of a BSN is governed by a combination of weights and biases, with the difference with ANNs being that BSN's activation function also includes a stochastical contribution.

A reasonable question here is: why molecular nanomagnets rather than any other magnetic nanoparticles? Firstly, with molecules we benefit from a systematization of data, which can allow experimentalists to choose the best system for their particular hardware implementation. Moreover, there is the issue of chemical and crystalline design of molecular nanomagnet-based nanoparticles vs superparamagnetic nanoparticles. Combining the SIMDAVIS dataset with inexpensive tools (such as MAGELAN)³⁹ one could check for crystals where the easy axis is perpendicular to a crystal plane, to facilitate choosing the direction of the easy axis in the device. But a further, more fundamental, advantage of molecular nanomagnets as LBNs is their reproducible magnetic behavior. Within the top-down approach of ferromagnetic nanoparticles, the magnetic dynamics vary with the size of the nanoparticle. The bottom-up approach of molecular nanomagnets guarantees reproducible magnetic dynamics that only depend on the chosen molecule. This would facilitate schemes that rely on specific operating frequencies, like lock-in amplification.

And how would the physics of molecular nanomagnets relate to the information processing as p-bits? At any given point in time, the state m_i of the ideal spin p-bit i is given by the signum of:

$$m_i = \text{sgn} \left(I_{i,[-1,1]} - r_{[-1,1]} \right) \quad (1)$$

where $I_{i,[-1,1]}$ is its input signal, normalized between -1 and 1, and $r_{[-1,1]}$ is a random number with a uniform distribution between -1 and +1, meaning that the output is stochastic but biased by the input. It is only unbiased when $I_i = 0$ and only deterministic when $I_i = 1$ or $I_i = -1$. For a spin p-bit, I_i can be embodied by the polarisation achieved by an external magnetic field B_i , i.e. a Zeeman effect that at a given temperature achieves a certain Boltzmann distribution. For the direction of the field corresponding to positive input signals, this is expressed as:

$$I_{i,[0,1]} = 2 \cdot \frac{e^{-E_{\text{Zeeman}}/kT}}{1 + e^{-E_{\text{Zeeman}}/kT}} \quad (2)$$

where

$$E_{\text{Zeeman}} = g\mu_B B M_J \quad (3)$$

where g is Landé's factor, μ_B is Bohr's magneton, B is the external magnetic field and M_J is the projection of the spin state. Applying B in the opposite direction would let one access the range $I_{i,[-1,0]}$. The same kind of biasing effect can be in principle achieved spintronically, by the flow of a spin-polarized current that acts as an effective magnetic field that couples with the spin p-bit.⁴⁰ In any case, the practical limit values of I_i , i.e. the saturation magnetisation, will be given by technological limits. In particular, large biases would require either very high effective magnetic fields or very low temperatures, or a combination of both. In the field of p-bits this behavior is often written, equivalently, as

$$I_{i,[-1,1]} = \tanh(H_i) \quad (4)$$

In the general case, for an interconnected network of p-bits, each input I_i results from the states of the rest of the p-bits m_j , weighted by their connections J_{ij} , plus a local bias h_i :

$$I_i = \sum_j J_{ij} m_j + h_i \quad (5)$$

Note that this fundamentally differs from the circuit model of Boolean logic gates that applies to conventional computing based on bits and quantum circuits employing qubits. Instead, it is closer to the way classical neural networks operate, with the difference being the stochastical character of p-bits. In a neural network, and also in a p-bit network, rather than a logical gate acting on a memory unit and altering it, the state of a given memory unit depends on the states of several other memory units with different weights, plus a bias (in the case of p-bits, to the bias one adds a random contribution). The system has to be adapted to solve a specific problem by adjusting the individual biases of each memory unit and the weights of each interaction between every pair of memory units, rather than by selecting an algorithm that applies a sequence of logical gates. This proposed use of molecular spin p-bits would add to recent proposals to employ molecular electric switches to emulate synaptic behaviour.⁴¹

2 Methods

We developed a custom implementation of Markov Chain Monte Carlo, which is based in random transitions for each spin at each time step and uses parameterised magnetization dynamics and Boltzmann distribution for the calculation of the Markov transition probabilities between the two possible spin states. In contrast with many Monte Carlo model implementations, our end goal is not to simulate the thermodynamic properties of a material via averaging of many samples but the dynamical behavior of a full population. Thus, within the many implementations of Markov Chain Monte Carlo methods (including Metropolis Monte Carlo), three crucial features for our goals are (a) we simulate independent particles, meaning we work with N identical and independent Markov chains, (b) instead of accumulating data over many runs with small sizes, we perform a single run with a large size, which will eventually be the actual number of magnetic molecules in our p-bit and (c) each calculation step has an associated natural time in real time units, which is taken into consideration for the calculation of the transition probabilities; this model is empirical and relies on externally determined relaxation parameters.

Assuming that the dynamics are the same for each individual nanomagnet and that the collective behaviour results from a simple addition of magnetic moment, one can employ the same τ to describe each individual spin. In particular, we employed the Maclaurin expansion of the exponential function to calculate the spin flip probability at a given time interval, and so allow recovering macroscopic spin dynamics of either a single and an ensemble of molecules. The magnetisation is simulated by the number of uncompensated spins and scaled to the experimental values (see full details in the SI section S1A).

In order to simulate stochastic spin dynamics in presence of a magnetic field, we introduced the Zeeman effect to produce a bias in the spin flip probability. This allows to recover Boltzmann statistics (see full details in SI section S1B). This complication of the model is necessary to be able to reproduce p-bit dynamics in a spin system that is driven by an external field.

All ac (alternate current) simulations were calculated with the same scheme, but under a time-dependent field. In-phase and out-of-phase susceptibilities were fitted employing a generalized Debye model (see full details in the SI section S2).

The screening of the SIMDAVIS dataset was performed by employing the SIMDAVIS dashboard (see full details in the SI sections S3, S4).¹⁸

All simulations presented herein were performed on a desktop computer and took, all in all, less than 24 h of processor time. The associated software to this work, named STOSS (for STOchastic Spin Simulator), and the instructions to reproduce all the graphic results are available at <https://github.com/gerlizg/STOSS>.

3 Results and discussion

3.1 Lanthanide-based, molecular, isolated spin p-bits at constant field

In state-of-the-art p-bit modelling, the spin dynamics caused by spin transfer torque effects on solid state superparamagnetic tunnel junctions are modeled by an Arrhenius/Neel-Brown ap-

proach.⁴² In the case of molecular spin p-bits, we benefit from the more sophisticated modelling of molecular nanomagnets, in which a commonly employed equation of the relaxation time (τ) reads as follows:

$$\tau^{-1} = \tau_{\text{QTM}}^{-1} + CT^n + \tau_0^{-1} \exp(-U_{\text{eff}}/T) \quad (6)$$

where the first term presents temperature-independent QTM, and the second and the third terms are thermally-assisted Raman and Orbach processes, respectively.

This relaxation time τ is employed to describe a collective behaviour. In particular, an ensemble of molecular nanomagnets experiences exponential decay of the magnetisation (see Figure 2):

$$M(t) = M_{\text{eq}} + (M_0 - M_{\text{eq}}) \exp[-(t/\tau)^\beta] \quad (7)$$

where M_{eq} and M_0 are the equilibrium and initial magnetisations, respectively; β is a so-called "stretching" parameter related to the time-dependent decay rate. Here we worked with $\beta = 1$, meaning independent spins (see details in the SI section S1), although STOSS can incorporate an averaged internal magnetic field reflecting the effect of dipolar coupling.

As a basic test for our simulator, we verified that, for a sufficiently large number of spins in the model, an exponential fit of the decay of the ensemble magnetisation recovers the input τ with the desired accuracy. This served as a basic benchmark of the model and also emphasized a further shortcoming: if the experimental magnetisation relaxes as a stretched exponential, our current model of independent spins cannot reproduce its shape properly. A simple modification of the code is available where the spin flip probability is a function of the spin up/down ratio, effectively simulating the average internal magnetic field created by dipolar interaction.

As an illustration, we employ our modelling software STOSS to simulate the magnetisation decay at three representative temperatures (2 K, 40 K, 80 K) with the parameters obtained experimentally in the case of $[(\text{Cp}^{\text{IPr5}})\text{Dy}(\text{Cp}^*)]^+$.²² Figure 2 upper panels depicts a simulation of the experimental results based on the evolution of $N = 10^5$ spins. While the simulation deviates significantly from the experimental decay curve at 2 K, they coincide well at high temperatures (40 K and 80 K). The deviation at low temperatures is due to the fact that the observed relaxation of magnetisation follows a stretched exponential decay ($0 < \beta < 1$ in Eq. 7), as occurs when spins are interacting. As a result, the value of β for 2 K is 0.5527, which differs greatly from the values found for 40 K and 80 K (0.9831 and 0.993, respectively). This variation is due to the time-dependent relaxation rate that likely stems from the redistribution of local dipolar fields when the magnetisation of the molecule is varied. In contrast, single exponential decay is normally adequate to account for the relaxation behaviour at high temperatures, as evidenced by $\beta \approx 1$ at 40 K and 80 K in this case. To prove that this is not a bulk simulation but rather intrinsically microscopic, the evolution of a smaller number of spins $N = 100$ at each temperature is shown in Figure 2 bottom panels. It is by the simple addition of a large number of these telegraph noises that the properties of the bulk sample are reproduced.

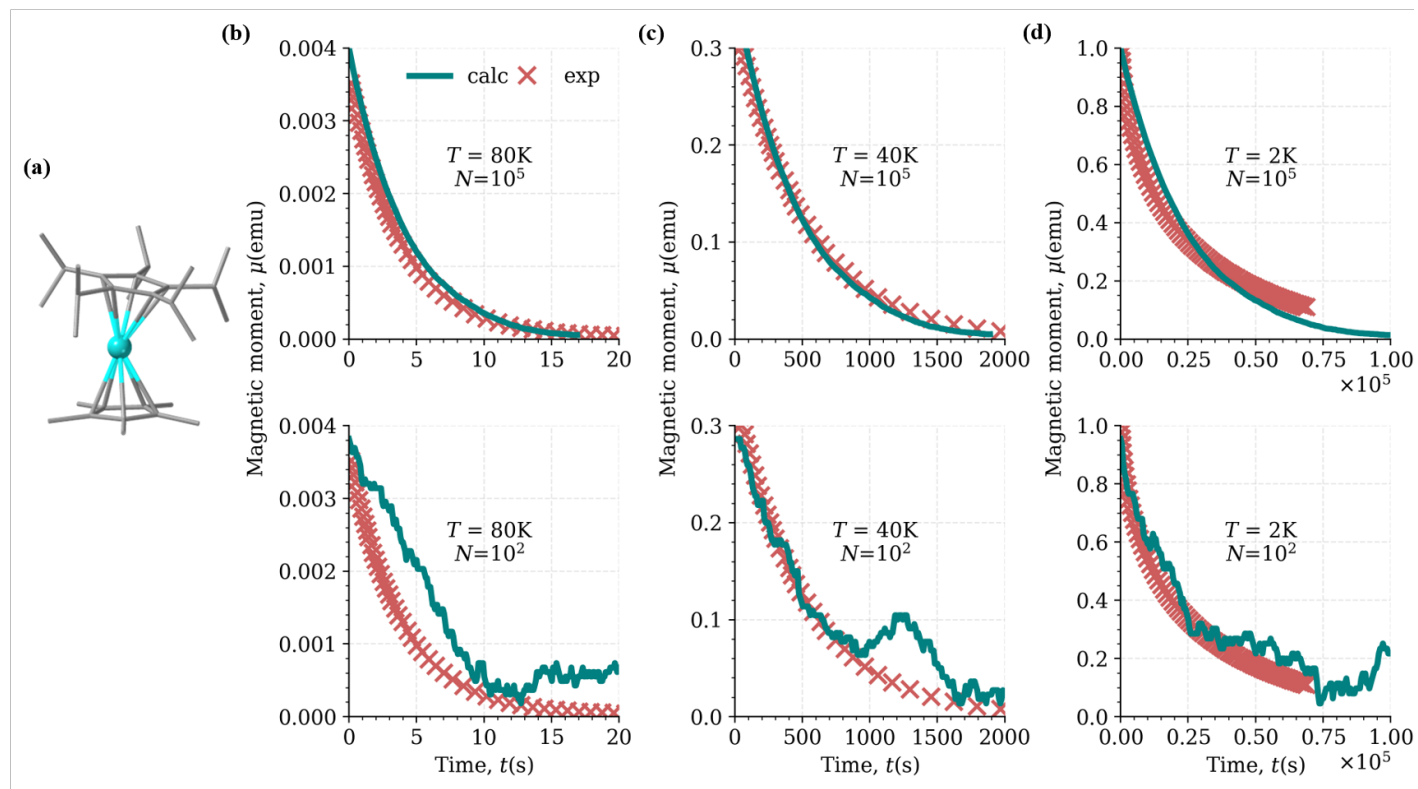


Fig. 2 (a) Structure of $[(\text{Cp}^{\text{iPr5}})\text{Dy}(\text{Cp}^*)]^+$ (Cp^{iPr5} , penta-iso-propylcyclopentadienyl; Cp^* , pentamethylcyclopentadienyl), (b-d, upper panels) its magnetisation decay vs time, experimental vs (scaled) simulation, at 3 temperatures, from left to right, 2K, 40K, 80K, with the simulations employing $N = 10^5$ spins. Experimental data are as extracted from Guo et al.²² The simulated magnetisation is plotted as difference between spins "up" and "down", starting from a fully polarized population, each evolving as explained in the text, and employing the parameters for Orbach, Raman and QTM mechanisms reported by Guo et al.²² (b-d, lower panels) present the same calculations, in the same conditions, but with a more limited number of spins $N = 10^2$ to evidence the stochastic nature of the model.

3.2 Lanthanide-based, molecular, dynamically driven spin p-bits

After simulating the spontaneous evolution of a single p-bit with constant input signal (e.g. constant magnetic field) and benchmarking the modelling software STOSS against the experimental relaxation of the magnetisation of a molecular nanomagnet, the second step is driving it with a time-dependent signal $I_i = f(t)$. The natural way to test the behaviour of the model in these conditions is by simulating the out-of-phase susceptibility of a molecular nanomagnet, where $I_i = \cos(t)$ (see Figure 3).

Note that microscopic (spin-by-spin) simulations of bulk ac behaviour are necessarily limited to low temperatures due to fundamental reasons. Indeed, the population difference between the distinct spin directions for very weak fields that are typical in ac susceptometry $B \leq 0.5$ mT is extremely small even at reasonably low temperatures in the order of $T = 2 - 4$ K, and the population difference gets even smaller at higher temperatures. This is the reason why it can be experimentally challenging to obtain ac signal for molecular nanomagnets that function at high temperatures. Furthermore, while sample sizes of the order of $m = 0.1$ mg are considered small, they typically contain a number of spins in the order of $N \simeq 10^{16}$, which is absolutely out of the bounds of what one can simulate microscopically. For this reason, we performed our simulation at $T = 20$ mK, a temperature in the

low limit of the experimentally accessible for researchers studying magnetic molecules. At this temperature, one should be able to access the spin dynamics corresponding to the QTM regime.

As above, the dynamic response is simulated by employing externally obtained parameters. For this simulation we chose $[\text{Dy}(\text{bath})(\text{tcpb})_3]$, where $\text{tcpb} = 1-(4\text{-chlorophenyl})-4,4,4\text{-trifluoro-1,3-butanedione}$ and $\text{bath} = 4,7\text{-diphenyl-1,10-phenanthroline}$, where $\tau_{\text{QTM}} = 0.067$ s, $n = 4.90$, $C = 7.80 \times 10^{-2} \text{ s}^{-1} \text{ K}^{-4.90}$, $\tau_0 = 2.83 \times 10^{-9}$ s, and the effective energy barrier (U_{eff}) is 116.87 cm^{-1} (167.87 K). In a first example simulation, we simulated 4 cycles with a period of an order of magnitude longer than τ_{QTM} . Employing $N = 10^4$ spins in the simulation, the response is largely in-phase with the magnetic field and yet a certain delay in the signal is already evident (see Figure 3(a) up). To offer a more intuitive insight into how this ensemble response signal is obtained, we also represented the same simulation with $N = 100$ spins (see Figure 3(a) down), where apparently there is just some relatively rapid telegraph noise overlapped with a slower random drift. It is crucial to understand that merely by summing a hundred similarly noisy patterns resulting from microscopic simulations one can reproduce a relatively clean macroscopic behaviour.

We repeated these calculations both at longer and shorter periods for the oscillation of the magnetic field and fitted the result to

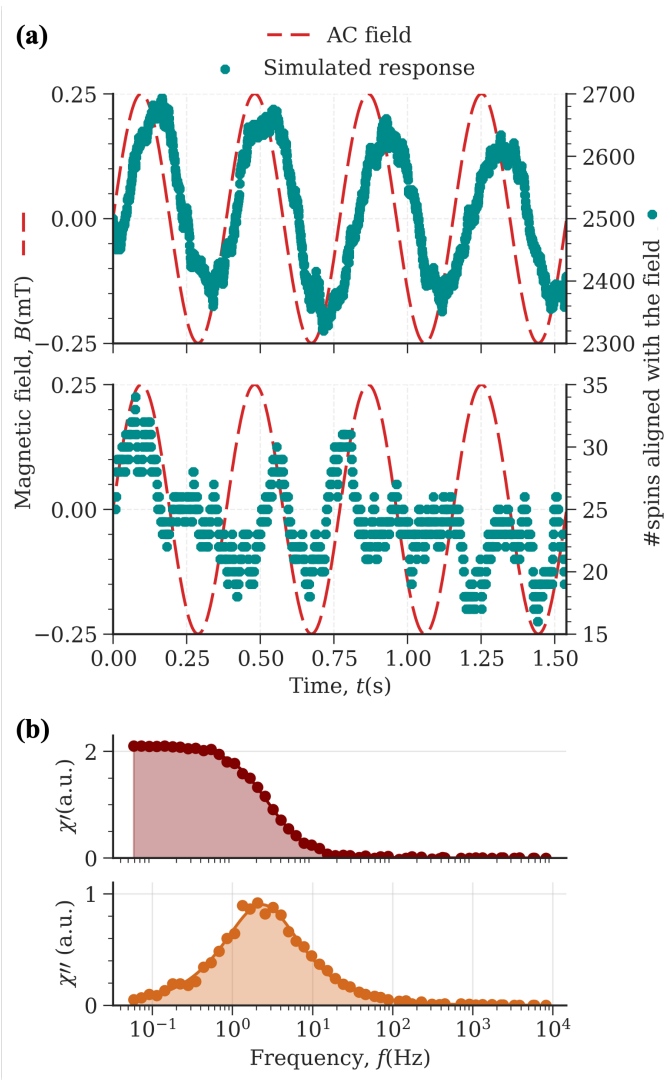


Fig. 3 Periodically driven p-bits, when simulated by our Markov Chain Monte Carlo calculations, behave qualitatively as spins in an ac susceptibility experiment: (a) calculated time evolution of $N = 2.5 \times 10^4$ (up) or $N = 50$ (down) stochastic spins described by the parameters corresponding to $[\text{Dy}(\text{bath})(\text{tcpb})_3]$, at 20 mK and under an external ac field of amplitude $B_{\text{max}} = 0.25$ mT and frequency 2 Hz that evidences a certain delay in the shape of the simulated magnetisation for $N = 2.5 \times 10^4$, whereas in the same conditions in the simulation of $N = 50$ stochastic spins neither the delay nor the periodicity are apparent and (b) simulated χ' , χ'' , where each value of χ' (χ'') corresponds to the prefactor of the $\cos(\sin)$ in a weighted $\sin+\cos$ fit of simulated oscillations for $N = 2.5 \times 10^4$ p-bits described by the parameters corresponding to $[\text{Dy}(\text{bath})(\text{tcpb})_3]$; the simulation was also performed at 20 mK meaning that the spin dynamics is governed by the parameter τ_{QTM} . The solid lines indicate the fits using the generalized Debye model.

a weighted sum of \sin and \cos functions to extract in-phase and out-of-phase signals (details in SI section S2A). The result, illustrated in Figure 3(b), is consistent with the expected behaviour, and the extracted τ of $5.79(6) \cdot 10^{-2}$ s using generalized Debye model is essentially identical to the experimental value.

In the context of molecular nanomagnets, STOSS should serve as an auxiliary tool in the ongoing effort for a proper interpretation of magnetic relaxation times and magnetic relaxation pa-

rameters.⁴³ In the context of p-bits, one can see this exercise as a synchronisation with an external periodic drive, but rather than being limited to simulating bulk ac experiments, one can easily think of ways to construct more sophisticated circuit architectures. With an adequate circuitry construction, the output of p-bit i can serve as input for p-bit j . To work at temperatures higher than $T = 20$ mT, it suffices to rise the applied magnetic field above $B = 0.5$ mT. Precisely this scenario is explored in the next section.

3.3 Lanthanide-based, molecular spin p-bit network

As a minimal toy model for a p-bit network, we explored a 2-p-bit architecture where each p-bit is constituted by the collective signal of 10^6 magnetic molecules, for example forming a thick layer on top of a sensor. We assume a circuit able to a spin excess of 10^3 spins, as should be possible to do employing nanoscale ($100 \text{ nm} \times 100 \text{ nm}$) Hall probes.⁴⁴ For simplicity we define as p-bit state 1 the case where there is a spin excess of 10^3 spins in the "up" direction, and 0 otherwise. Compared with requiring also a spin excess for the 0 state, this means that 0 and 1 states are slightly asymmetrical, but it saves us from having to consider "dead" times where neither an excess of spin "up" nor "down" can be detected. Also for simplicity, we take identical p-bits in terms of τ .

We allowed a free evolution for the spin dynamics of p-bit i (no input signal, no bias, $B_i = 0$). It was also assumed that each p-bit flip in p-bit i is detected by a sufficiently fast readout and it is used to switch the magnetic field acting on p-bit j . We chose two systems from the SIMDAVIS dataset which presented distinct advantages and a maximum in the out-of-phase signal around 4 K and 40 K respectively. Thus, for the simulations at $T = 4$ K we chose $[\text{Dy}\{\eta^4\text{-C}_4(\text{SiMe}_3)_4\}\eta^4\text{-C}_4(\text{SiMe}_3)_3\text{-k}-(\text{CH}_2\text{SiMe}_2)_2]^{2-}$ molecules⁴⁵, which are air stable and thus in principle easier to process. This system presents a $\tau_0 = 1.83 \times 10^{-9}$ s and $U_{\text{eff}} = 464$ K. For the simulations at $T = 40$ K we chose quadruple decker $\{[\text{Dy}(\text{obPc})_2]\text{Cd}[\text{Dy}(\text{obPc})_2]\}$ molecules⁴⁶, where obPC = 2,3,9,10,16,17,23,24-octabutoxyphthalocyaninato. This is a phthalocyaninato-based system that should be easy to deposit on surfaces with a predictable orientation of the easy axis of magnetization. This system presents a $\tau_0 = 1.2 \times 10^{-7}$ s and $U_{\text{eff}} = 30.24$ K. At both temperatures we employed an "on" field (B_j) of 20 mT. The "off" field was fitted so that the average field cancels over a long experiment. In this case, the information flow is unidirectional, but both the scheme and the modelling are scalable to larger networks and to more complex information feedbacks.

To quantify the association between the values of the two pbits, we consider the four states (0,0), (0,1), (1,0), (1,1) where the first and second index correspond to the state of p-bit i and j respectively, and $N(i,j)$ as the number of such states in a continuous run of the simulation. We define the association ϕ between p-bit i and p-bit j as:

$$\phi = \frac{N(0,0) \cdot N(1,1) - N(0,1) \cdot N(1,0)}{\sqrt{N_{1*} \cdot N_{0*} \cdot N_{*0} \cdot N_{*1}}} \quad (8)$$

with

$$N_{1*} = N(1,0) + N(1,1) \quad (9)$$

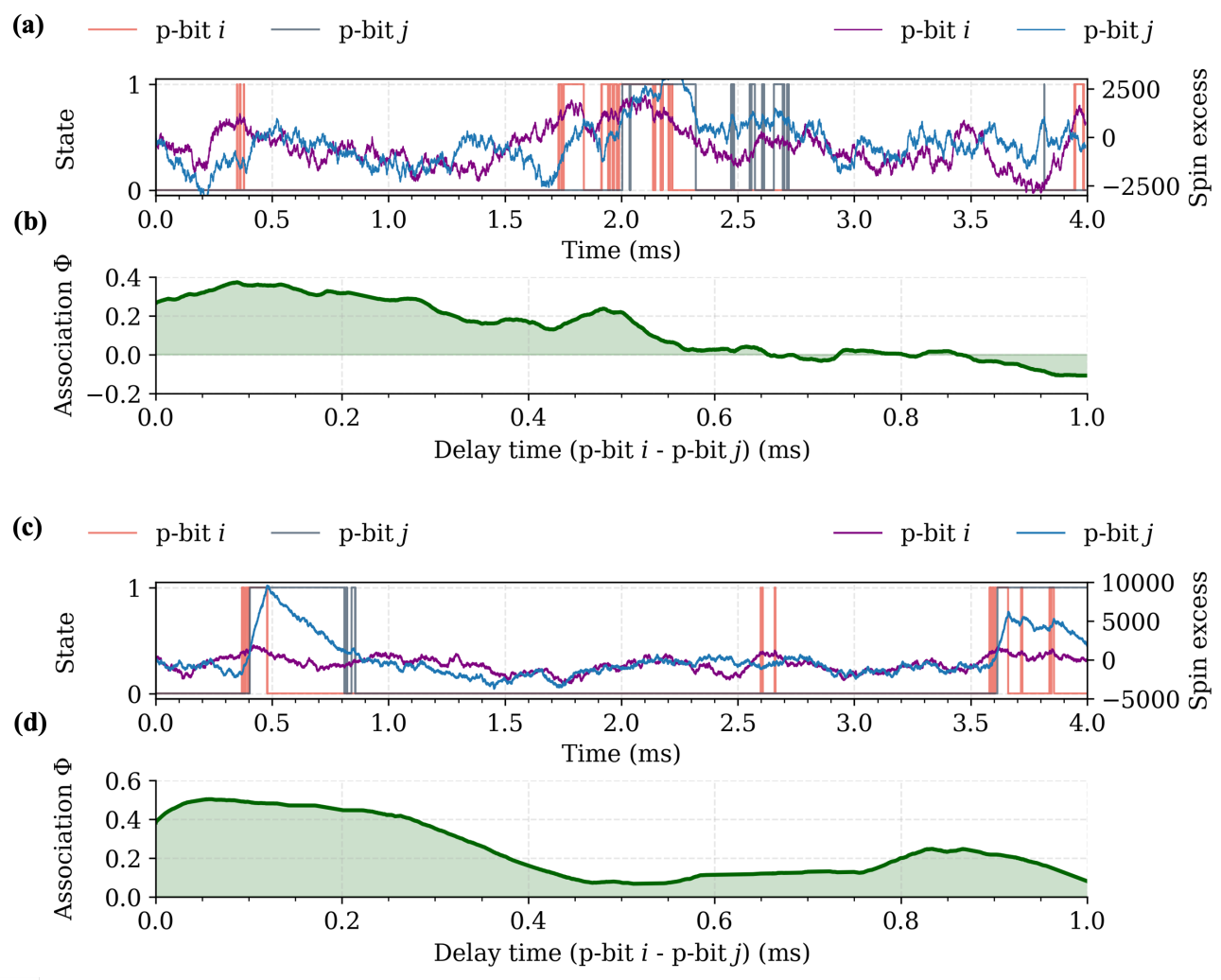


Fig. 4 Scheme for a toy network of associated p-bits based on the collective behavior of (a,b) $[\text{Dy}\{\eta^4\text{-C}_4(\text{SiMe}_3)_4\}\eta^4\text{-C}_4(\text{SiMe}_3)_3\text{-k-(CH}_2\text{SiMe}_2\text{)}^2\text{-}]$ molecules⁴⁵ at $T = 4$ K and (c,d) quadruple decker $\{[\text{Dy}(\text{obPc})_2]\text{Cd}[\text{Dy}(\text{obPc})_2]\}$ molecules⁴⁶ at $T = 40$ K, where the state of p-bit i controls a magnetic field $B = 0.02$ T acting on p-bit j . (a,c): State of p-bit i and p-bit j vs time; one can appreciate that after a period where p-bit i takes the value 1 (or 0), p-bit j often follows. (b,d) Association ϕ (see equation 8) comparing the state of p-bit i at a certain time with state of p-bit j after a certain delay time where the x-axis is the delay time.

$$N_{0*} = N(0,0) + N(0,1) \quad (10)$$

$$N_{*0} = N(0,0) + N(1,0) \quad (11)$$

$$N_{*1} = N(0,1) + N(1,1) \quad (12)$$

By choosing relatively cold temperatures, even moderate fields and a moderate number of magnetic molecules per pbit are able to achieve a strong association between the p-bits (see Figure 4).

We also calculated the delayed association by considering the state of p-bit i at a certain time t_0 and the state of p-bit j at a later time $t_0 + d$. What one observes both here and also for a single spin as a p-bit in Supplementary Figure S6 is a base instantaneous correlation, that is initially enhanced by allowing a short delay time between the stimulus and the response, to accommodate the intrinsic dynamics, and which is then gradually lost for longer delay times, until only noise around $\phi \simeq 0$ is observed, i.e. mathematically independent values of p-bits i and j . One can also

appreciate that the same magnetic field $B = 0.02$ T that has an adequate effect at 40 K is excessive at 4 K, with the spin excess of p-bit j overshooting by a wide margin and taking a long time to recover when the state of p-bit i changes.

How could such a p-bit network be implemented in practice? We revealed a possibility in Figure 1(b). Each p-bit would sit on a clover-type Hall effect probe, where a current is passed in one direction and a Hall voltage is measured in the perpendicular direction, so that the sign of the Hall voltage is controlled by the sign of the magnetic moment in the p-bit. This output voltage signal then needs to be amplified and converted into a current. This current, passing through an electromagnet, generates a magnetic field B that acts as input (red arrow) to another p-bit, with a sign that depends on the value of the first p-bit. A magnetic field $B = 0.02$ T is realistic if the response time is wanted to be relatively short and able to react to the change in the state of the p-bits. Note the crucial effect of the magnetic field here, creating

a Zeeman splitting strong enough to allow our microscopic simulator to pick up correlations at a temperature of 40 K instead of requiring an extreme cryogenic temperature of 20 mK like in the previous section.

What we extract from these simulations is that at 4 K and 40 K even with a moderate number of $M = 10^6$ magnetic molecules one can expect a very high association between p-bits communicated by reasonable magnetic fields ($\simeq 0.02$ T) and times ($\simeq 1$ ms). Simulations would be more challenging at 300 K, higher number of molecules and slower nanomagnets would be required, but one can expect these results to carry over to room temperature. In the next section we discuss the chemical design of the desired characteristic relaxation times.

3.4 Experimental constraints and SIMDAVIS dataset screening for p-bit behaviour

The most convenient setup, from the point of view of the technical requirements, involves working at room temperature (RT). This should also be a short-term goal for scalable technologies, especially if one takes energy consumption into consideration. However, this seems yet out of the question with molecular nanomagnets employed either in traditional computation as bits or in quantum computation as spin qubits. For both applications, stochastic spin flips that happen at non-cryogenic temperatures are detrimental and need to be avoided. Then, working at RT would require long relaxation/coherence times, and this in turn would require a combination of an extremely high relaxation barrier and extremely weak spin-phonon coupling. These demands have not been achieved yet with molecular nanomagnets and it remains unclear whether they can ever be achieved.

The situation is completely different for p-bits, where stochastic spin flips are expected and a mandatory part of the information processing. In this case the electronic equipment needs to operate at least as fast as the relaxation time of the p-bit. If the equipment operates at significantly lower frequency than the p-bit, only an average signal would be recorded and the stochasticity would be lost. Very slow p-bits are also not practical, since the overall operating speed of the device will be determined by the slowest among the p-bit relaxation time and the electronic equipment. The ideal is an approximate match in terms of speed between the p-bits and the read-write capabilities of the electronic equipment one is using. If e.g. the electronics are able to read and write at 1 kHz, then one wants to work with a molecular nanomagnet presenting a relaxation time $\tau \simeq 1$ ms at the working temperature.

The translation of these requirements to the parameters characterizing the spin dynamics of molecular nanomagnets is surprising. One does not actually need or desire particularly high values of the effective barrier U_{eff} , which is, shockingly for the molecular nanomagnet community, not necessarily a key parameter. If one operates at 300 K, which is often close to the high temperature limit, spin relaxation time is given in a good approximation by the attempt time, τ_0 . Assuming, that is, that Raman relaxation does not overtake the Orbach process (but why should it, given that Orbach's thermal dependence is stronger?). In that scenario, the goal is to find highly processable molecular systems with a value

of τ_0 that is compatible with the available electronics. Should one need to operate at lower temperatures, the goal will be to find the molecule presenting a response time in the desired time range.

We estimated $\tau_{300\text{K}}$ as the characteristic relaxation time according to the Néel-Arrhenius equation at 300 K for the 612 samples for which there is U_{eff} and τ_0 information in the SIMDAVIS dataset (see Figure 5 upper panel).¹⁸ Here we focus on the two most relevant chemical categories to classify molecular nanomagnets, namely the lanthanoid ion and the chemical family. We show with violin plots the fact that, while there is a large dispersion in $\tau_{300\text{K}}$ values there is also an influence from the metal ion, from the chemical family, and from their combinations. Still, it is evidenced that the three most popular ions for molecular nanomagnet design generally require very fast operating times to act as p-bits at room temperature. The analogous plot for $\tau_{4\text{K}}$ can be seen in the Figure 5 lower panel. In this case we discarded all samples with $U_{\text{eff}} > 50$ K to avoid plotting impractically (and in many cases, unrealistically) long relaxation times.

A thorough study of the influence of different chemical variables on $\tau_{300\text{K}}$ and $\tau_{4\text{K}}$ is available in the Supplementary Information Sections S3 and S4. We found that for the chemical design of molecular spin p-bits that are slow enough to be operable at reasonable frequencies and at room temperature, one could lean towards coordination spheres consisting of nine donor atoms in a mixture of Oxygen and Nitrogen, stemming from 3 ligands, and probably choosing a lanthanide ion other than Dy^{3+} , Tb^{3+} or Er^{3+} . Embodying each p-bit in larger ensembles of molecular spins would further facilitate working at manageable speeds and temperatures (see Supplementary Information Section S2).

As discussed in the previous section and depicted in Figure 4(b), achieving a significant correlation between single spins at moderate magnetic fields such as $B = 0.2$ T requires relatively low temperatures as in the order of 40 K. However, if one desires to work at RT, the signal will be too weak, but this is true in any case where one employs a single molecule. Much stronger signals, allowing one to pick up much weaker correlations, will arise from a large collection of molecular nanomagnets acting as a single p-bit. Indeed, note that Boltzmann populations are governed by the ratio between energy difference and working temperature. This means that, if one were to use similar sensitivity and sample sizes as in the case of commercial ac susceptometry, a $B = 0.02$ T (3 orders of magnitude higher than regular ac field) would allow obtaining sufficient population difference at temperatures up to 3 orders of magnitude higher than in an ac experiment. In this case, would mean being able to quantify correlation at temperatures much higher than 300 K. Ultimately, the practical temperature limit and sample requirement will depend on the experimental implementation.

4 Conclusions

We employed STOSS, a microscopic simulator code for spin p-bits based on molecular nanomagnets, to explore this potential emergent technological application, distinct from conventional bits and from quantum qubits. To test the software, we reproduced the most characteristic macroscopic magnetic dynamics of molecular nanomagnets, namely magnetisation relaxation

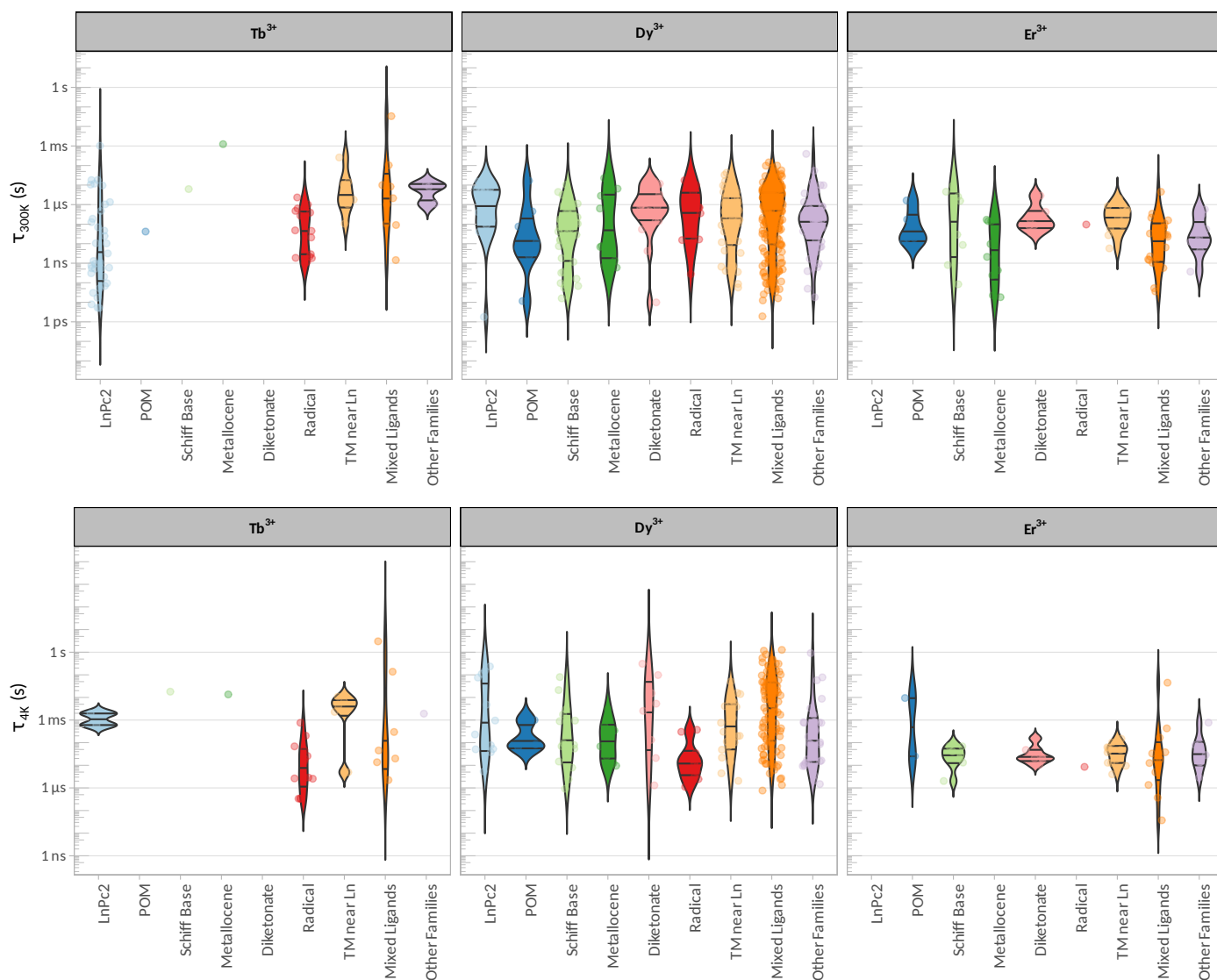


Fig. 5 Estimated relaxation times at room temperature (τ_{300K}) and at 4 K (τ_{4K}) for molecular nanomagnets based on Tb^{3+} , Dy^{3+} , Er^{3+} represented as violin plots. Relaxation times are categorised for the main chemical families considered in the SIMDAVIS dataset.¹⁸ The Néel-Arrhenius equation was used to estimate this parameter. The violin plot outlines illustrate kernel probability density, i.e. the width of the coloured area represents the proportion of the data located there. Further complementary representations employing other categorisation criteria are available in the SI.

and in-phase, out-of-phase susceptometry, by simulating the individual states in a collective of spin p-bits. With the help of STOSS, we found that under realistic conditions it should be technologically possible to build small networks of p-bits based on molecular nanomagnets. We found an inverse correlation between room temperature p-bit performance and molecular nanomagnets performance. This is unsurprising considering (a) U_{eff} is a good predictor of molecular nanomagnet behavior and (b) the approximate proportionality $\tau_0^{-1} \propto U_{eff}^3$.^{18,47} In this aspect, these Low Barrier Nanomagnets are proposed to build the basic neuronal units of Artificial Stochastic Neural Networks. Since molecular single ion magnets and spin qubits have been explored for decades,⁴⁸ this new potential application starts already with a wealth of molecular diversity, theoretical tools and systematically organised data facilitating statistical and machine learning studies.^{18,49,50} This gives magnetic molecules the potential to be

screened, chosen, and adapted to the different technological constraints of different possible implementations. Here one needs to acknowledge that despite the continuous efficiency improvements in the information and communications technology sector, it has been shown that there is an increasing weight of computing-related emission in the climate crisis, a problem which cannot be addressed merely by technical advances based on futuristic modes of information processing.⁵¹ However, we believe that research on molecular nanomagnets as probabilistic information carriers is of sufficient fundamental interest to merit further exploration.

Data availability

All custom data generated and employed for this study are available at <https://github.com/gerlizg/STOSS>.

Code availability

The code named STOSS (for STOchastic Spin Simulator) is available at <https://github.com/gerlitzg/STOSS>. The instructions to reproduce all the graphic results are in the Supporting Information Section S5 and at <https://github.com/gerlitzg/STOSS>.

Author Contributions

GMGF: (for all except 3.4) investigation, methodology, software and validation; (for 3.1 and 3.3) formal analysis; writing. SGS: (for 3.2) software and validation; (for all except 3.4) visualisation. ZH: (for 3.2) formal analysis; writing. LER: conceptualisation; writing; (for 3.4) software, investigation, formal analysis and visualisation. SCS: conceptualisation, supervision and writing. AGA: conceptualisation and supervision, project administration, funding acquisition and writing.

Conflicts of interest

There are no conflicts to declare

Acknowledgements

L.E.R., S.G.S., S.C.S. and A.G.A. have been supported by the COST Action MolSpin on Molecular Spintronics (Project 15128). A.G.A. and Z.H. thank funding from European Union (EU) Programme Horizon 2020 (FATMOLS project), and A.G.A. also thanks Generalitat Valenciana (GVA) CIDEGENT/2021/018 grant. S.C.S. acknowledges funding from the European Research Council (ERC) in EU Horizon 2020 grant agreement ERC-2017-AdG-788222 “MOL2D”. S.C.S., S.G.S. and L.E.R. gratefully acknowledge support from the Spanish Ministerio de Ciencia e Innovación (MICINN) grant PID2020-117264GB-I00, and A.G.A. thanks MICINN PID2020-117177GB-I00 grant (both MICINN grants co-financed by FEDER funds). S.G.S. acknowledges MICINN PRE2018-083350 grant related to MINECO CTQ2017-89528-P project. S.C.S. acknowledges Excellence Unit María de Maeztu CEX2019-000919-M funding. L.E.R. gratefully acknowledges support from GVA PROMETEO/2019/066. This study forms part of the Quantum Communication program and was supported by MICINN with funding from European Union NextGenerationEU (PRTR-C17.I1) and by GVA (QMol COMCUANTICA/010).

Notes and references

- 1 F. Madaeni, K. Chokmani, R. Lhissou, H. Saeid, Y. Gauthier and S. Tolszczuk-Leclerc, *The Cryosphere*, 2022, **2022**, 1447.
- 2 S. Robert, S. Büttner, C. Röcker and A. Holzinger, *Reasoning Under Uncertainty: Towards Collaborative Interactive Machine Learning*, Springer International Publishing AG, New York, NY, USA, 2016.
- 3 C. N. Mohamed Derbeli and O. Barambones, *Mathematics*, 2021, **2021**, 2068.
- 4 H. Wang and Y. Xuan, *Remote Sensing*, 2022, **2022**, 3823.
- 5 A. Sonia, K. Kumar and C. Iwendi, *Sustainability*, 2022, **2022**, 15292.
- 6 B. Brown and H. Card, *IEEE Transactions on Computers*, 2001, **50**, 891–905.
- 7 T. Tuma, A. Pantazi, M. Le Gallo, A. Sebastian and E. Eleftheriou, *Nature Nanotechnology*, 2016, **11**, 693–699.
- 8 A. Chanthbouala, V. Garcia, R. O. Cherifi, K. Bouzehouane, S. Fusil, X. Moya, S. Xavier, H. Yamada, C. Deranlot, N. D. Mathur *et al.*, *Nature materials*, 2012, **11**, 860–864.
- 9 M. A. Nielsen and I. Chuang, *Quantum computation and quantum information*, 2002.
- 10 S. Chowdhury, A. Grimaldi, N. A. Aadit, S. Niazi, M. Mohseni, S. Kanai, H. Ohno, S. Fukami, L. Theogarajan, G. Finocchio, S. Datta and K. Y. Camsari, *IEEE Journal on Exploratory Solid-State Computational Devices and Circuits*, 2023, 1–1.
- 11 J. Kaiser and S. Datta, *Applied Physics Letters*, 2021, **119**, 150503.
- 12 K. Y. Camsari, S. Chowdhury and S. Datta, *Phys. Rev. Appl.*, 2019, **12**, 034061.
- 13 J. Kaiser and S. Datta, *Appl. Phys. Lett.*, 2021, **119**, 150503.
- 14 W. A. Borders, A. Z. Pervaiz, S. Fukami, K. Y. Camsari, H. Ohno and S. Datta, *Nature*, 2019, **573**, 390–393.
- 15 A. Mizrahi, N. Locatelli, R. Lebrun, V. Cros, A. Fukushima, H. Kubota, S. Yuasa, D. Querlioz and J. Grollier, *Scientific Reports*, 2016, **6**, 30535.
- 16 N. Locatelli, A. Mizrahi, A. Accioly, R. Matsumoto, A. Fukushima, H. Kubota, S. Yuasa, V. Cros, L. G. Pereira, D. Querlioz, J.-V. Kim and J. Grollier, *Phys. Rev. Appl.*, 2014, **2**, 034009.
- 17 S. Kanai, K. Hayakawa, H. Ohno and S. Fukami, *Phys. Rev. B*, 2021, **103**, 094423.
- 18 Y. Duan, J. T. Coutinho, L. E. Rosaleny, S. Cardona-Serra, J. J. Baldoví and A. Gaita-Ariño, *Nat. Commun.*, 2022, **13**, 7626.
- 19 A. Gaita-Ariño, F. Luis, S. Hill and E. Coronado, *Nat. Chem.*, 2019, **11**, 301–309.
- 20 M. R. Wasielewski, M. D. Forbes, N. L. Frank, K. Kowalski, G. D. Scholes, J. Yuen-Zhou, M. A. Baldo, D. E. Freedman, R. H. Goldsmith, T. Goodson III *et al.*, *Nature Reviews Chemistry*, 2020, **4**, 490–504.
- 21 S. Giménez-Santamarina, S. Cardona-Serra, J. M. Clemente-Juan, A. Gaita-Ariño and E. Coronado, *Chem. Sci.*, 2020, **11**, 10718–10728.
- 22 F.-S. Guo, B. M. Day, Y.-C. Chen, M.-L. Tong, A. Mansikkamäki and R. A. Layfield, *Science*, 2018, **362**, 1400–1403.
- 23 C. A. Gould, K. R. McClain, D. Reta, J. G. Kragoskow, D. A. Marchiori, E. Lachman, E.-S. Choi, J. G. Analytis, R. D. Britt, N. F. Chilton *et al.*, *Science*, 2022, **375**, 198–202.
- 24 C. Godfrin, A. Ferhat, R. Ballou, S. Klyatskaya, M. Ruben, W. Wernsdorfer and F. Balestro, *Phys. Rev. Lett.*, 2017, **119**, 187702.
- 25 M. Atzori and R. Sessoli, *Journal of the American Chemical Society*, 2019, **141**, 11339–11352.
- 26 D. Aguilà, L. A. Barrios, V. Velasco, O. Roubeau, A. Repollés, P. J. Alonso, J. Sesé, S. J. Teat, F. Luis and G. Aromí, *Journal of the American Chemical Society*, 2014, **136**, 14215–14222.
- 27 A. Ardavan, A. M. Bowen, A. Fernandez, A. J. Fielding, D. Kaminski, F. Moro, C. A. Muryn, M. D. Wise, A. Ruggi, E. J. L. McInnes, K. Severin, G. A. Timco, C. R. Timmel, F. Tuna, G. F. S. Whitehead and R. E. P. Winpenny, *npj Quantum Information*, 2015, **1**, 15012.
- 28 I. Gimeno, W. Kersten, M. C. Pallarés, P. Hermosilla, M. J. Martínez-Pérez, M. D. Jenkins, A. Angerer, C. Sánchez-Azqueta, D. Zueco, J. Majer, A. Lostao and F. Luis, *ACS Nano*, 2020, **14**, 8707–8715.
- 29 S. Carretta, D. Zueco, A. Chiesa, Á. Gómez-León and F. Luis, *Applied Physics Letters*, 2021, **118**, 240501.
- 30 D. Aravena and E. Ruiz, *Dalton Trans.*, 2020, **49**, 9916–9928.
- 31 S. Takamatsu, T. Ishikawa, S. Y. Koshihara and N. Ishikawa, *Inorganic Chemistry*, 2007, **46**, 7250–7252.
- 32 J. Liu, E. Del Barco and S. Hill, *Physical Review B - Condensed Matter and Materials Physics*, 2012, **85**, 012406.
- 33 J. Long, B. G. Shestakov, D. Liu, L. F. Chibotaru, Y. Guari, A. V. Cherkasov, G. K. Fukin, A. A. Trifonov and J. Larionova, *Chem. Commun.*, 2017, **53**, 4706–4709.
- 34 M. Briganti, F. Santanni, L. Tesi, F. Totti, R. Sessoli and A. Lunghi, *Journal of the American Chemical Society*, 2021, **143**, 13633–13645.
- 35 L. Gu and R. Wu, *Physical Review Letters*, 2020, **125**, 117203.
- 36 A. Lunghi and S. Sanvito, *The Journal of Chemical Physics*, 2020, **2020**, 174113.
- 37 O. Hassan, R. Faria, K. Y. Camsari, J. Z. Sun and S. Datta, *IEEE Magnetics Letters*, 2019, **10**, 1–5.
- 38 B. Sutton, R. Faria, L. A. Ghantasala, R. Jaiswal, K. Y. Camsari and S. Datta, *IEEE Access*, 2020, **8**, 157238–157252.
- 39 N. F. Chilton, D. Collison, E. J. L. McInnes, R. E. P. Winpenny and A. Soncini, *Nature Communications*, 2013, **4**, 2551.
- 40 N. Locatelli, V. Cros and J. Grollier, *Nature Materials*, 2014, **13**, 11–20.
- 41 Y. Wang, Q. Zhang, H. P. A. G. Astier, C. Nickle, S. Soni, F. A. Alami, A. Borriani, Z. Zhang, C. Honnigfort, B. Braunschweig, A. Leoncini, D.-C. Qi, Y. Han, E. del Barco, D. Thompson and C. A. Nijhuis, *Nature Materials*, 2022, **21**, 1403–1411.
- 42 D. Vodenicarevic, N. Locatelli, A. Mizrahi, T. Hirtzlin, J. S. Friedman, J. Grollier and D. Querlioz, 2018 IEEE International Symposium on Circuits and Systems (ISCAS), 2018, pp. 1–4.
- 43 D. Reta and N. F. Chilton, *Phys. Chem. Chem. Phys.*, 2019, **21**, 23567–23575.

- 44 D. Collomb, P. Li and S. J. Bending, *Scientific Reports*, 2019, **9**, 14424.
- 45 B. M. Day, F.-S. Guo, S. R. Giblin, A. Sekiguchi, A. Mansikkamäki and R. A. Layfield, *Chemistry – A European Journal*, 2018, **24**, 16779–16782.
- 46 K. Katoh, Y. Horii, N. Yasuda, W. Wernsdorfer, K. Toriumi, B. K. Breedlove and M. Yamashita, *Dalton Trans.*, 2012, **41**, 13582–13600.
- 47 A. Abragam and B. Bleaney, *Electron Paramagnetic Resonance of Transition Ions*, Oxford University Press, 2012.
- 48 N. F. Chilton, *Annual Review of Materials Research*, 2022, **52**, 79–101.
- 49 V. H. A. Nguyen and A. Lunghi, *Phys. Rev. B*, 2022, **105**, 165131.
- 50 A. Lunghi and S. Sanvito, *Nature Reviews Chemistry*, 2022, **6**, 761–781.
- 51 B. Knowles, *ACM TechBrief: Computing and Climate Change*, 2021.